

High-bandwidth optical magnetometer

Ricardo Jiménez-Martínez,^{1,2,*} W. Clark Griffith,¹ Svenja Knappe,¹ John Kitching,¹ and Mark Prouty³

¹Time and Frequency Division, National Institute of Standards and Technology, Boulder, Colorado 80305, USA

²Department of Physics, University of Colorado, Boulder, Colorado 80309, USA

³Geometrics Inc., 2190 Fortune Drive, San Jose, California 95131, USA

*Corresponding author: jimenezm@nist.gov

Received July 3, 2012; revised October 17, 2012; accepted October 23, 2012;
posted October 24, 2012 (Doc. ID 171654); published November 28, 2012

We demonstrate a scalar ^{87}Rb optical magnetometer that retains magnetic-field sensitivities below $10\text{pT}/\sqrt{\text{Hz}}$ over 3 dB bandwidths of 10 kHz in an ambient field $B_o = 11.4\ \mu\text{T}$ and using a measurement volume of $1\ \text{mm}^3$. The magnetometer operates at high atomic densities where both the sensitivity and the bandwidth are limited by spin-exchange collisions between the alkali atoms. By operating in this regime, our measurements show that the bandwidth of the magnetometer can be increased without a significant degradation in its sensitivity.

OCIS codes: 020.0020, 130.6010, 300.6210.

1. INTRODUCTION

It is well established that optically polarized alkali-metal atoms in the vapor phase offer one of the most sensitive means for the measurement of magnetic fields [1]. Two important performance characteristics of optical magnetometers are their sensitivity and their bandwidth, which in broad terms are set by the spin-coherence time of the polarized atoms. Better sensitivities are achieved by suppressing spin decoherence [2], but generally at the cost of lower bandwidth. There are some applications that could benefit from a magnetometer that has a high bandwidth. For instance, one important application for optically pumped atomic scalar magnetometers [1] is the detection of magnetic anomalies, such as those originating from buried unexploded ordnance (UXO) [3–5]. In order to accurately identify a buried UXO, it is helpful to gather a dense array of DC magnetic field readings using an optical magnetometer. Additional information can be gained from AC electromagnetic fields scattered off the object at a frequency around 10 kHz, which is usually detected with an array of pick-up coils [3]. This approach is often not implemented due to the high cost of collecting both data types [5]. In addition, current platforms [3] having both types of sensors are bulky and cannot be used in areas where space restriction is an issue. Having a single sensor, highly miniaturized and portable, capable of performing both types of measurements with the sensitivity and bandwidth (on the order of 10 kHz) of current devices, would greatly help to simplify and reduce the costs of the measurement process.

Previous work [6,7] has shown that the bandwidth of optical magnetometers can be extended beyond its natural 3 dB cutoff frequency with external feedback by using a large gain in the feedback loop. However, in this case the noise in the feedback loop increases, which in turn degrades the sensitivity [6]. Another approach performs continuous quantum non-demolition measurements with spin-projection noise-limited spectroscopy [8]; this approach has reached sensitivities of $22\ \text{fT}/\sqrt{\text{Hz}}$ with 2 kHz bandwidth. A third approach is that of introducing spin decoherence mechanisms such as power broadening or atomic collisions [1]. In particular, spin-

exchange collisions between alkali atoms is a well-known source of linewidth broadening that has the interesting property that the strength of the detected signal increases with the alkali density and hence improves as the linewidth is broadened. This approach offers a simple and straightforward route to increase the natural bandwidth of the magnetometer without degrading sensitivity. Furthermore, it is very amenable for highly miniaturized and portable devices such as chip-scale optical magnetometers, where the optical path length is small and therefore where an increase in alkali density is particularly useful.

To explore this regime, we studied the sensitivity and bandwidth of a scalar Bell–Bloom optical magnetometer [9] as a function of atomic density. We show that by operating in the regime where spin decoherence is dominated by spin-exchange collisions between the alkali atoms, one can achieve large bandwidths while preserving high sensitivity. Specifically, for our experimental conditions, the magnetometer achieves bandwidths ranging from 1 to 10 kHz while preserving sensitivities below $10\ \text{pT}/\sqrt{\text{Hz}}$, limited by technical noise, in an ambient field $B_o = 11.4\ \mu\text{T}$. Higher bandwidths can be achieved by operating at higher atomic densities and higher magnetic fields. The magnetometer is implemented with a simple setup that can be miniaturized using slight variations of chip-scale atomic devices [10–13].

2. THEORY

Scalar optically pumped alkali-metal magnetometers are based on the precise measurement of the precession frequency of the atomic spins in a magnetic field (B_o). This precession frequency is the Larmor frequency $\omega_o = \gamma B_o$, where $\gamma = 2\pi \times 7\ \text{Hz/nT}$ for the ^{87}Rb alkali atoms used in our setup. When the atoms are driven at the Larmor frequency, for instance in the Bell–Bloom magnetometer by modulating the optical pumping rate [9], they all precess in phase with the driving field and a large macroscopic magnetization results, which can be detected with a probe beam (see Fig. 1). The atoms also experience a variety of decoherence processes that cause their spin precession to deviate from a perfect

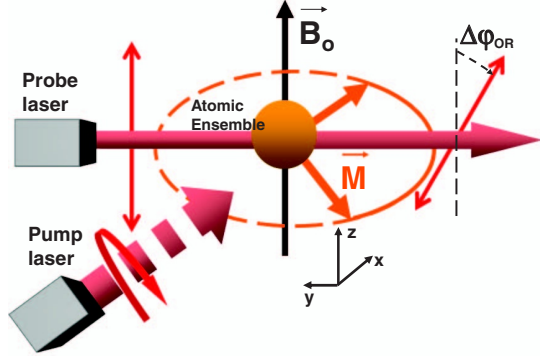


Fig. 1. (Color online) Basic configuration of the Bell-Bloom magnetometer. A circularly polarized laser beam pumps the atomic ensemble, which acquires a macroscopic magnetization (M). In the presence of a magnetic field B_0 , M precesses about the field at Larmor frequency. Readout of the precession frequency is implemented by OR detection of a linearly polarized laser beam. Continuous readout is achieved by modulating the amplitude of the pumping light.

sinusoidal motion. The rate and magnitude of the decoherence processes can be characterized by a coherence time T_2 (transverse spin relaxation time), which determines the width of the resonance in the frequency domain.

The coherence time determines both the sensitivity and the bandwidth of the magnetometer. The sensitivity (in $T/\sqrt{\text{Hz}}$) can be expressed as

$$\delta B = \frac{1}{\gamma} \frac{1}{T_2 S/N}, \quad (1)$$

where S/N is the signal-to-noise ratio with the noise expressed per unit bandwidth. Thus, for a fixed signal-to-noise ratio, longer coherence times imply a higher magnetometer sensitivity [2]. The bandwidth, on the other hand, is determined by the spectrum of the atomic response and therefore by the resonance width $\Delta\nu_{\text{HWHM}} = 1/(2\pi T_2)$ [1].

In the following sections, we investigate how the magnetometer bandwidth and sensitivity scale with the alkali atomic density, in the regime where the coherence time is dominated by spin-exchange collisions.

A. Magnetometer Bandwidth

In this work, the enhancement in magnetometer bandwidth is achieved by increasing the spin-relaxation rate ($\Gamma_2 = 1/T_2$) through alkali-alkali spin-exchange collisions. The spin-exchange collision rate is given by

$$R_{\text{SE}} = n\sigma_{\text{SE}}\bar{v}, \quad (2)$$

n being the alkali atomic density, where $\sigma_{\text{SE}} \approx 1.9 \times 10^{-14} \text{ cm}^2$ is the spin-exchange cross section [14] for alkali atoms, and \bar{v} is the average relative velocity of the colliding alkali atoms, equal to $\bar{v} \approx 4 \times 10^4 \text{ cm/s}$ for ^{87}Rb at 130°C .

An expression for the width (HWHM) of the magnetic line, and thus the magnetometer bandwidth, is given by [15]

$$\Delta\nu_{\text{HWHM}} = \frac{1}{2\pi} \Gamma_2 = \frac{1}{2\pi} \left(\frac{R_{\text{SE}}}{q_{\text{SE}}} + \Gamma_o + \frac{(R_p + R_{\text{pr}})}{q} \right), \quad (3)$$

where R_p and R_{pr} are the pumping rate due to the time-averaged pump light and probe light, respectively, and Γ_o is

the relaxation due to other mechanisms (for instance, spin depolarization due to collisions of the alkali atoms with cell walls and buffer-gas atoms). The factors q and q_{SE} appearing in Eq. (3) correspond to the nuclear slowing-down factors due to the coupling of the electronic spin with the nuclear spin, which acts as a reservoir of spin orientation. The first factor q is given by $q = 2I + 1$, where I is the nuclear spin of ^{87}Rb . In the limit where $R_{\text{se}} \ll \omega_o$, $q_{\text{SE}} = 3(2I + 1)^2 / (2I(2I - 1))$ [15,16]. The modulated pump-light intensity results in a time-dependent pumping rate $R(t) = R_p(1 + \cos(\omega t))$, with R_p being the time-averaged pumping rate.

In the limit where the decoherence is dominated by spin-exchange relaxation, we can see from Eq. (3) that the resonance linewidth, and therefore the magnetometer bandwidth, is proportional to R_{SE} and therefore to the alkali density n .

B. Magnetometer Sensitivity in the High-Atomic-Density Regime

At a fundamental level the sensitivity is limited by spin-projection noise [1]. At high atomic densities, in the limit where the spin relaxation is dominated by spin-exchange collisions, the sensitivity due to spin-projection noise (in $T/\sqrt{\text{Hz}}$) is given by $\delta B_{\text{spn}} = \frac{1}{\gamma} \sqrt{(\sigma_{\text{SE}}\bar{v})/V}$ [2]. In our setup the probed volume is approximately 1 mm^3 ; thus this sensitivity is on the order of $40 \text{ fT}/\sqrt{\text{Hz}}$ [17].

Other sources of fundamental noise (photon shot noise) and technical noise (such as electronic noise and noise in the amplitude and frequency of the probe light [18,19]) limit the sensitivity of the magnetometer. Here, we focus only on the sensitivity limited by photon shot noise. In this section, we present the main results of our analysis, while the details are covered in Appendix A.

The signal is obtained by measuring the optical rotation (OR) angle ϕ_{OR} of a linearly polarized probe (see Fig. 1). Using the balanced polarimeter in Fig. 2, the signal is acquired by subtracting the photocurrents I_1 and I_2 of the two photodetectors and is given, in the limit of small rotation angle, by [15,20] $S_{\text{OR}} = 2I_t\phi_{\text{OR}}$, where $I_t = I_1 + I_2$. We consider the case where the optical line is homogeneously broadened by atomic collisions with buffer-gas atoms (in our experiment the width of the pressure-broadened D1 optical line is approximately 25 GHz) such that the hyperfine structure is not resolved. When the drive frequency is equal to the Larmor frequency, ϕ_{OR} is given by (see Appendix A)

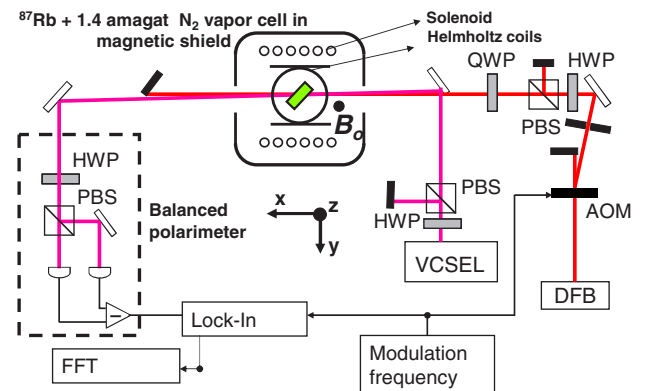


Fig. 2. (Color online) Experimental setup. PBS, polarizing beam-splitter; HWP, half-wave plate; QWP, quarter-wave plate; and FFT, spectrum analyzer.

$$\phi_{\text{OR}} = \frac{1}{4} \text{OD}_o M_o \frac{\Gamma_p}{\Gamma_2} \left(\frac{x}{1+x^2} \right), \quad (4)$$

where OD_o is the on-resonance optical depth, M_o is the polarization degree in zero magnetic field along the probe propagation axis, $\Gamma_p = R_p/q$, and $x = (\nu_L - \nu_o)/(\Delta\nu/2)$ is the normalized detuning of the probe laser frequency ν_L . The shot noise in the OR angle is given in $\text{rad}/\sqrt{\text{Hz}}$ by

$$\delta\phi_{\text{OR}} = \sqrt{\frac{\text{OD}_o}{2\eta R_{\text{pr}} n V (1+x^2)}}, \quad (5)$$

where η is the quantum efficiency of the photodetectors.

We calculate the signal-to-noise ratio $S/N = \phi_{\text{OR}}/\delta\phi_{\text{OR}}$; then inserting this result as well as the relaxation rate from Eq. (3) into Eq. (1), we arrive at the following expression for the sensitivity due to photon shot noise:

$$\delta B_{\text{psn}} = \frac{2\Gamma_2^2}{\gamma\Gamma_p M_o} \sqrt{\frac{2}{\eta\text{OD}_o n V R_{\text{pr}}}} x^{-1} (1+x^2)^{1/2}. \quad (6)$$

For a far detuned probe ($x \gg 1$), Eq. (6) is similar to the photon shot-noise sensitivity derived in [20], but takes into account an optically driven spin precession for which the transverse polarization is not equal to unity, but is instead equal to $(1/2)(\Gamma_p/\Gamma_2)M_o$.

From Eq. (6), assuming $R_{\text{pr}} \ll R_p$, one can see that the sensitivity is optimized when the broadening due to the pumping light is approximately $R_{\text{SE}}/q_{\text{SE}} + \Gamma_o$. In this case, one can also see that in the limit where the spin relaxation is dominated by spin-exchange collisions and for $x \gg 1$, the sensitivity becomes $\delta B_{\text{psn}} \approx R_{\text{SE}}(\gamma M_o \sqrt{\eta\text{OD}_o n V R_{\text{pr}}})^{-1}$ and thus is independent of atomic density if the probe pumping rate is constant. In principle, further optimization could be achieved by choosing R_{pr} such that the photon shot noise equals spin-projection noise; at this point the sensitivity would be a factor $\sqrt{2}$ larger than the one calculated for δB_{psn} above.

3. EXPERIMENTAL SETUP

The experimental setup is shown in Fig. 2, and is centered around a micromachined vapor cell with a $2 \text{ mm} \times 1 \text{ mm} \times 1 \text{ mm}$ cavity filled with enriched ^{87}Rb and 1.4 amagat of N_2 buffer gas. Due to the high buffer-gas pressure, the hyperfine structure of ^{87}Rb is not resolved; the measured width (FWHM) of the optical line is $\Delta\nu \approx 25 \text{ GHz}$. The cell is heated by running electrical current at 370 kHz through four chip resistors mounted on each of the cell windows; the operating temperature ranges approximately between $80 \text{ }^\circ\text{C}$ and $180 \text{ }^\circ\text{C}$. By adjusting the temperature, the on-resonance optical depth (OD_o) was varied between 0.05 and 16, from which we estimate that the atomic density was varied between 10^{12} cm^{-3} and $4.5 \times 10^{14} \text{ cm}^{-3}$. The cell is placed inside a magnetic shield and tilted with respect to the light propagation axis to prevent etalon effects.

A circularly polarized pump beam, originating from a distributed feedback laser, pumps the atoms along the x -direction (see Fig. 2). The pump light is tuned to the center of the pressure-broadened D1 optical transition of ^{87}Rb at 795 nm and is amplitude modulated at ω_o with an acousto-optic modulator. The magnetic field B_o is generated along

the z -direction by a Helmholtz coil. A second Helmholtz coil and a solenoid reduce residual DC fields along x and y .

The polarization of the atomic ensemble is probed by measuring the OR of the transmitted probe light originating from a vertical-cavity surface-emitting laser. The detuning of the optical frequency of the probe from the D1 line is adjusted to maximize the magnetometer signal. For our experimental setup, we found that when $\text{OD}_o \ll 1$, the optimum detuning is approximately $\Delta\nu/2$, whereas for $\text{OD}_o > 1$, it is roughly $\sqrt{\text{OD}_o}(\Delta\nu/2)$. For all the measurements reported here, the probe power was kept constant at a level of $12 \text{ } \mu\text{W}$. The polarization of the transmitted probe light is analyzed by use of a balanced polarimeter. The cross section for both pump- and probe-light beams inside the vapor cell is $A \approx 0.6 \text{ mm}^2$, mostly limited by the vapor-cell aperture; their path length is $l \approx 1.4 \text{ mm}$, which yields an effective measurement volume of about 1 mm^3 .

A lock-in amplifier demodulates the polarimeter signal at the modulation frequency of the pump (80 kHz). The lock-in time constant and roll-off of the lock-in amplifier were set to $10 \text{ } \mu\text{s}$ and 6 dB/octave, respectively. Magnetic resonance signals are generated by slowly ramping the transverse magnetic field (B_o) about resonance ($11.4 \text{ } \mu\text{T}$) and recording the dispersive signal obtained [see inset in Fig. 3(b)] from one of the lock-in outputs upon proper adjustment of its phase. The recorded signal is then fitted to a dispersive Lorentzian, from which its slope on resonance, amplitude, and width is obtained. The noise in the dispersive signal is measured with

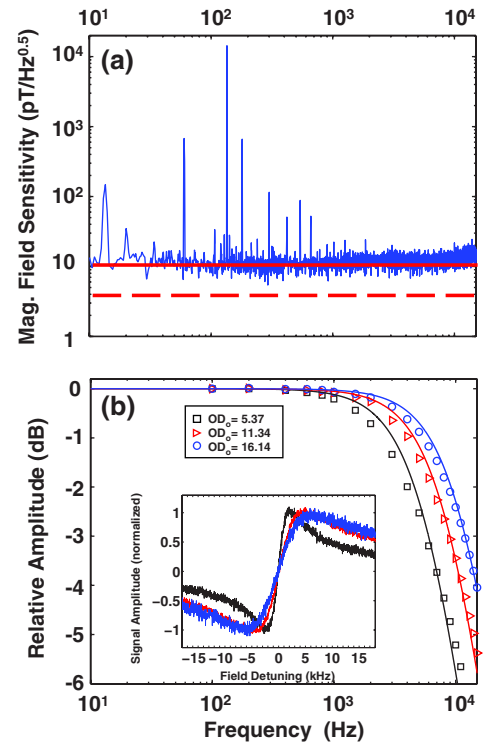


Fig. 3. (Color online) (a) Noise spectra of the lock-in signal converted to units of magnetic field. The ambient field is $11.4 \text{ } \mu\text{T}$, $\text{OD}_o \approx 16$, and the magnetic linewidth (HWHM) is 11 kHz . Solid and dashed curves correspond to the measured noise $10 \text{ pT}/\sqrt{\text{Hz}}$ and photon shot noise $4 \text{ pT}/\sqrt{\text{Hz}}$, respectively. (b) Frequency response of the magnetometer; solid curves are used to guide the eye. Inset: magnetic resonances at very low pumping light levels at the given OD_o .

a fast-Fourier-transform spectrum analyzer when the static magnetic field is tuned on resonance [Fig. 3(a)]. To measure the frequency response of the magnetometer, a small oscillating field is superimposed on B_0 and its frequency is varied between 100 Hz and 15 kHz. The amplitude of the resulting peaks in the frequency spectrum of the signal is then measured [Fig. 3(b)]. The ambient field B_0 and the corresponding precession frequency were chosen based on our lock-in amplifier, which operates up to 100 kHz. We expect that the upper limit in the magnitude of the field to be measured will be determined by the point at which the nonlinear Zeeman effect causes a splitting equal to the resonance width.

4. RESULTS AND DISCUSSION

A. Power-Broadening Optimization

The interplay among magnetic resonance linewidth, signal-to-noise, and magnetometer sensitivity can be observed in Fig. 4, which shows these parameters for our magnetometer as a function of pumping power at low optical depths ($OD_0 \approx 0.1$). Linear power broadening of the resonance is observed, while the signal-to-noise ratio saturates. This overall behavior explains the magnetic-field sensitivity observed in Fig. 4(b). It is observed that the optimum sensitivity is achieved when the pumping power broadens the line to a level of 1 kHz, which is about twice the residual broadening extrapolated to zero power.

From the measured linewidth reported in Fig. 4(a), we estimate an extrapolated zero-light power width of 400 Hz. From the measured optical depth, we infer an atomic density $n = 3 \times 10^{12} \text{ cm}^{-3}$. At this atomic density, the estimated

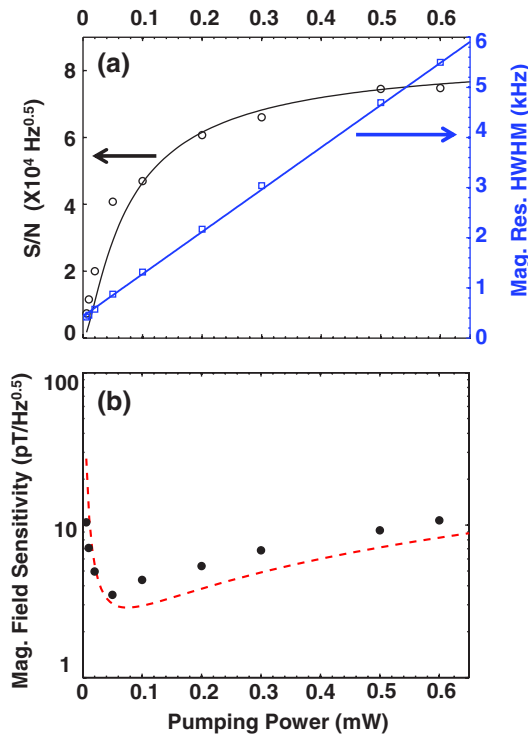


Fig. 4. (Color online) (a) Magnetic resonance width (HWHM) and measured S/N as a function of pumping power. (b) Magnetic field sensitivity as a function of pumping power at $OD_0 = 0.13$. Solid lines in (a) serve to guide the eye. The dashed line in (b) corresponds to the estimated photon shot-noise sensitivity using Eq. (6).

broadening of the line due to spin-exchange collisions is 49 Hz; thus the extrapolated width at zero-light power is dominated by other relaxation mechanisms. From this observation, we infer that $\Gamma_o/(2\pi)$, in Eq. (3), is approximately 350 Hz.

B. Magnetometer Sensitivity and Resonance Linewidth Versus On-Resonance Optical Depth

We show in Fig. 5 the magnetic resonance width, the measured OR angle, and the measured noise as a function of on-resonance optical depth.

In Fig. 5(a), the hollow and filled symbols represent the width (HWHM) of the resonance for the light power optimized as described above and the extrapolated width at zero-light power, respectively. The solid line in Fig. 5(a) corresponds to the contribution from spin-exchange collisions, as calculated by Eqs. (2) and (3), with the nuclear slow-down factor

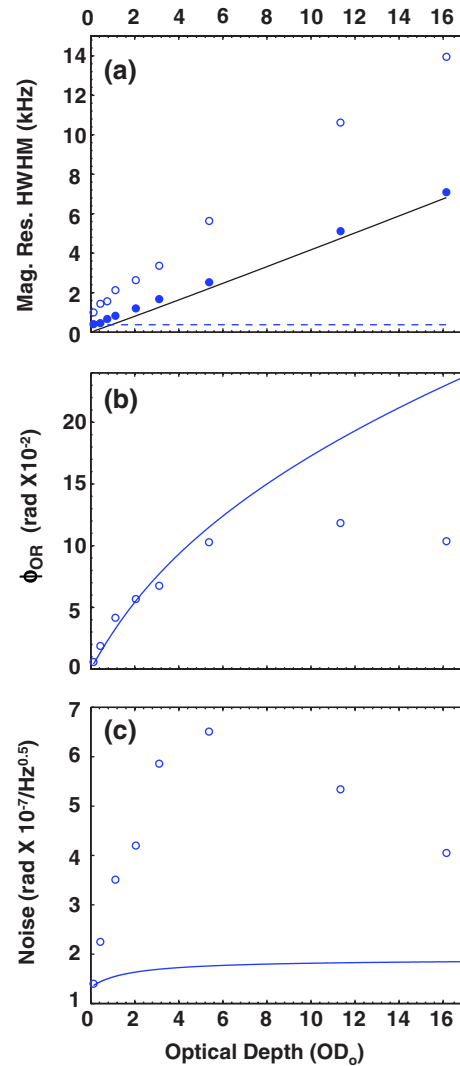


Fig. 5. (Color online) (a) Magnetic linewidth, (b) OR angle, and (c) noise as a function of on-resonance optical depth. In (a), the hollow and solid symbols correspond to the width (HWHM) of the resonance line and extrapolated zero-light level, respectively, whereas the solid line is the relaxation contribution from spin-exchange collisions. In (b) and (c) the solid lines correspond to the expected OR angle and shot noise according to Eqs. (4) and (5), respectively. See text for details.

q_{SE} stated above, while the dashed line indicates the value of $\Gamma_o/2\pi$.

The measured OR angle is shown in Fig. 5(b). Two regimes are observed. When $OD_o \ll 1$, the probe detuning is roughly at $\Delta\nu/2$ from the optical line, as described above. Here the cell is optically thin, with the result that the OR angle increases roughly linearly with OD_o . As the resonant optical depth increases beyond unity, we reach a second regime. Here, to avoid large optical absorption, the probe field is detuned at a level $\sqrt{OD_o}(\Delta\nu/2)$. Thus, in this regime the measured OR angle no longer increases linearly with OD_o , but instead as $\sqrt{OD_o}$. The solid line in Fig. 5(b) corresponds to the OR angle as predicted by Eq. (4) assuming that $\Gamma_p = R_{SE}/q_{SE} + \Gamma_o$, a spin polarization fraction $M_o = 0.5$, and a probe detuning as outlined above. In general good quantitative agreement is found between Eq. (4) and the data points, with the trends at low and high values of OD_o described above reproduced. The last two data points in Fig. 5(b) deviate from the theory estimates. One possible reason for this is that the operation at large optical densities introduces difficulties in creating a uniform spin polarization throughout the vapor cell, which in turn degrades signal strength. The problem of nonuniform spin polarization can be mitigated to some extent through the use of two counterpropagating pumping beams [21] or hybrid optical pumping [22].

The noise in the OR angle is shown in Fig. 5(c). Here the points represent the measured noise and the solid line is the shot-noise estimate from Eq. (5) assuming $\eta = 0.75$, and a pumping rate $R_{pr} = R_o \exp(-OD_o(1+x^2)^{-1})/(1+x^2)$ with a detuning as described above, and $R_o = 1.9 \times 10^3 \text{ s}^{-1}$, which corresponds to the pumping rate for the power and beam size of our probe on resonance with the optical line and for $OD_o \ll 1$.

The sensitivity as a function of on-resonance optical depth is shown in Fig. 6. Here the points correspond to the measured sensitivity, and the solid line is the estimate obtained from Eq. (6) with the values for its parameters given above. In general, the measured sensitivity remains below $10 \text{ pT}/\sqrt{\text{Hz}}$ for the entire range of optical depths.

In the limit where the spin relaxation is dominated by spin-exchange collisions and for a far-detuned probe, Eq. (6) predicts that the sensitivity should be independent of atomic density if the probe pumping rate R_{pr} is constant. However, in the solid line in Fig. 6, we observe a degradation in the sensitivity with optical depth (for $OD_o > 1$), which is due to the fact that all of the measurements and estimates reported here

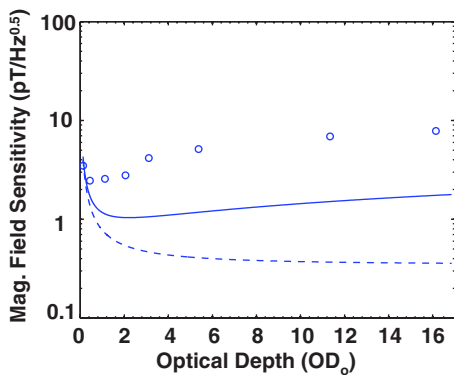


Fig. 6. (Color online) Magnetic-field sensitivity as a function of on-resonance optical depth. See text for details.

were carried out at a constant probe light power and with the probe detuning adjusted to optimize the signal. If instead the probe power were increased to compensate for the increased detuning at large optical depths in such a way to keep R_{pr} a constant, the magnetometer sensitivity is expected to reach a constant value in the limit of high OD_o . This projected sensitivity is shown in the dashed line in Fig. 6. To generate this line we used the same parameters used to generate the solid line but assumed a constant $R_{pr} = 950 \text{ s}^{-1}$.

In summary, our results in Figs. 4, 5, and 6 show that for the optimum pumping rate one can enlarge the resonance line-width by increasing the atomic density of the alkali atoms, and thus increasing spin-exchange relaxation, while only modestly affecting the sensitivity. It is important to emphasize that in order for the sensitivity and bandwidth to be determined by spin-exchange relaxation, the Larmor frequency must be much larger than the spin-exchange relaxation rate. Otherwise spin-exchange relaxation broadening is suppressed [16], which in turn improves sensitivity at the cost of reduced bandwidth.

5. CONCLUSIONS

In conclusion, we have shown a scalar optical magnetometer that achieves bandwidths ranging from 1 to 10 kHz in a 1 mm^3 probe volume, while preserving sensitivities below $10 \text{ pT}/\sqrt{\text{Hz}}$, limited by technical noise. Higher bandwidths can be achieved by operating at higher atomic densities while retaining optimized sensitivity. Compared to SQUID magnetometers [23], which have demonstrated bandwidths much larger than 10 kHz, optical magnetometers can be highly miniaturized and portable. In addition, they could be manufactured at low cost since they do not need cryogenic cooling [10–13]. These properties make the magnetometer presented here very attractive in applications requiring miniaturized, portable, magnetic sensors with a bandwidth on the order of 10 kHz, for instance in the detection of UXO [3–5].

We believe our magnetometer is very amenable for miniaturization. A small (vapor cell volume $\approx 7 \text{ cm}^3$), portable, fiber-coupled, optical magnetometer using OR detection and two independent, copropagating, pump- and probe-light beams is reported in [24]. An implementation of this magnetometer using a 1 mm^3 micromachined vapor cell seems feasible, particularly with the recent development of fiber-coupled chip-scale atomic magnetometers [12,13].

APPENDIX A

In the following derivation for the magnetometer sensitivity in the limit of photon shot noise, we adapt the approach of [14,20] to a Bell-Bloom magnetometer [9]. The signal obtained from the balanced polarimeter in Fig. 2 is obtained by subtracting the photocurrents I_1 and I_2 of the two photodetectors and is given by [15,25]

$$S_{OR} = I_t \sin(2\phi_{OR}), \quad (\text{A1})$$

where $I_t = I_1 + I_2 = \Re P_t$, with P_t and \Re being the transmitted light power and the photodetector's responsivity, respectively. In the limit where the optical line is homogeneously broadened by atomic collisions with buffer-gas atoms such that the hyperfine structure is not resolved, ϕ_{OR} is given by [20]

$$\phi_{\text{OR}} = \frac{1}{2} \sigma'_o n l M_x \left(\frac{x}{1+x^2} \right), \quad (\text{A2})$$

where M_x is the spin polarization degree of the ^{87}Rb vapor along the probe propagation axis, and $\sigma'_o = 2r_e c f / \Delta\nu$ corresponds to the pressure-broadened absorption cross section for the ^{87}Rb D1 transition on resonance [15]. Here r_e is the classical electron radius and f is the oscillator strength.

To obtain the projection of the spin polarization M_x , we need to solve the equations of motion of the spin system depicted in Fig. 1. We follow the phenomenological approach of Bell and Bloom [9], which consists in solving the Bloch equations explicitly for this system [9]. Ignoring DC and off-resonant components, one can show [9] that on resonance ($\omega = \omega_o$), M_x is given by

$$M_x = M_o \frac{\Gamma_p}{2\Gamma_2} \cos(\omega t). \quad (\text{A3})$$

Inserting this expression into Eq. (A2), we arrive at Eq. (4), where $\text{OD}_o = \sigma'_o n l$.

The photon shot noise in the polarimeter signal is $N_{\text{psn}} = 2I_t \delta\phi_{\text{OR}}$. Here, the shot noise in the rotation angle is given by [14,15,20,25]

$$\delta\phi_{\text{OR}} = \frac{1}{2\sqrt{\eta\Phi_{\text{pr}}t}}, \quad (\text{A4})$$

where Φ_{pr} is the photon flux in the probe light reaching the photodetectors, and t is the measurement time. We follow [14,20] in expressing the photon flux of the transmitted probe light in terms of its pumping rate R_{pr} , which is given by [14]

$$R = \frac{\Phi}{A} \sigma'_o \left(\frac{1}{1+x^2} \right), \quad (\text{A5})$$

where A is the transverse area of the beam interacting with the alkali atoms. Then, we can express $\Phi_{\text{pr}} = R_{\text{pr}} n V (1+x^2) / \text{OD}_o$. Inserting this result in Eq. (A4), and assuming $t = 1/(2\text{BW})$ [20] and a bandwidth of 1 Hz, we arrive at Eq. (5).

We can then calculate the signal-to-noise ratio in the limit of small rotation angle ($\sin(2\phi_{\text{OR}}) \approx 2\phi_{\text{OR}}$): $S/N = S_{\text{or}}/N_{\text{psn}} = \phi_{\text{OR}}/\delta\phi_{\text{OR}}$. Finally inserting this result as well as the decoherence rate from Eq. (3) into Eq. (1), we arrive at Eq. (6).

ACKNOWLEDGMENTS

The authors thank Rahul Mhaskar and Ethan Pratt for helpful comments on the manuscript. R. Jimenez acknowledges support from the Roberto Rocca Education Program. This work is a contribution of the National Institute of Standards and Technology (NIST), an agency of the U.S. government, and is not subject to copyright.

REFERENCES

1. D. Budker and M. Romalis, "Optical magnetometry," *Nat. Phys.* **3**, 227–234 (2007).
2. J. C. Allred, R. N. Lyman, T. W. Kornack, and M. V. Romalis, "High-sensitivity atomic magnetometer unaffected by spin-exchange relaxation," *Phys. Rev. Lett.* **89**, 130801 (2002).
3. H. H. Nelson and J. R. McDonald, "Multisensor towed array detection system for UXO detection," *IEEE Trans. Geosci. Remote Sens.* **39**, 1139–1145 (2001).
4. S. D. Billings, "Discrimination and classification of buried unexploded ordnance using magnetometry," *IEEE Trans. Geosci. Remote Sens.* **42**, 1241–1251 (2004).
5. S. Billings, F. Shubitidze, L. Pasion, L. Beran, and J. Foley, "Requirements for unexploded ordnance detection and discrimination in the marine environment using magnetic and electromagnetic sensors," in *Proceedings of OCEANS 2010 IEEE-Sidney* (IEEE, 2010), p. 18.
6. P. D. D. Schwindt, L. Hollberg, and J. Kitching, "Self-oscillating rubidium magnetometer using nonlinear magneto-optical rotation," *Rev. Sci. Instrum.* **76**, 126103–4 (2005).
7. J. M. Higbie, E. Corsini, and D. Budker, "Robust, high-speed, all-optical atomic magnetometer," *Rev. Sci. Instrum.* **77**, 113106–7 (2006).
8. V. Shah, G. Vasilakis, and M. V. Romalis, "High bandwidth atomic magnetometry with continuous quantum nondemolition measurements," *Phys. Rev. Lett.* **104**, 013601 (2010).
9. W. E. Bell and A. L. Bloom, "Optically driven spin precession," *Phys. Rev. Lett.* **6**, 280 (1961).
10. P. D. D. Schwindt, S. Knappe, V. Shah, L. Hollberg, J. Kitching, L.-A. Liew, and J. Moreland, "Chip-scale atomic magnetometer," *Appl. Phys. Lett.* **85**, 6409–6411 (2004).
11. P. D. D. Schwindt, B. Lindseth, S. Knappe, V. Shah, J. Kitching, and L.-A. Liew, "Chip-scale atomic magnetometer with improved sensitivity by use of the Mx technique," *Appl. Phys. Lett.* **90**, 081102–3 (2007).
12. J. Preusser, V. Gerginov, S. Knappe, and J. Kitching, "A micro-fabricated photonic magnetometer," in *Proceedings of the IEEE Sensors Conference* (IEEE, 2008), p. 344.
13. S. Knappe, T. H. Sander, O. Kosch, F. Wiekhorst, J. Kitching, and L. Trahms, "Cross-validation of microfabricated atomic magnetometers with superconducting quantum interference devices for biomagnetic applications," *Appl. Phys. Lett.* **97**, 133703 (2010).
14. M. P. Ledbetter, I. M. Savukov, V. M. Acosta, D. Budker, and M. V. Romalis, "Spin-exchange-relaxation-free magnetometry with cs vapor," *Phys. Rev. A* **77**, 033408 (2008).
15. S. J. Seltzer, "Developments in alkali-metal atomic magnetometry," Ph.D. thesis (Princeton University, 2008).
16. W. Happer and A. C. Tam, "Effect of rapid spin exchange on the magnetic-resonance spectrum of alkali vapors," *Phys. Rev. A* **16**, 1877–1891 (1977).
17. V. Shah, S. Knappe, P. D. D. Schwindt, and J. Kitching, "Subpicotesla atomic magnetometry with a microfabricated vapour cell," *Nat. Photonics* **1**, 649–652 (2007).
18. J. C. Camparo, "Conversion of laser phase noise to amplitude noise in an optically thick vapor," *J. Opt. Soc. Am. B* **15**, 1177–1186 (1998).
19. R. Jiménez-Martínez, S. Knappe, W. C. Griffith, and J. Kitching, "Conversion of laser-frequency noise to optical-rotation noise in cesium vapor," *Opt. Lett.* **34**, 2519–2521 (2009).
20. I. M. Savukov, S. J. Seltzer, M. V. Romalis, and K. L. Sauer, "Tunable atomic magnetometer for detection of radio-frequency magnetic fields," *Phys. Rev. Lett.* **95**, 063004 (2005).
21. W. C. Griffith, S. Knappe, and J. Kitching, "Femtotesla atomic magnetometry in a microfabricated vapor cell," *Opt. Express* **18**, 27167–27172 (2010).
22. M. V. Romalis, "Hybrid optical pumping of optically dense alkali-metal vapor without quenching gas," *Phys. Rev. Lett.* **105**, 243001 (2010).
23. D. Drung, H. Matz, and H. Koch, "A 5-MHz bandwidth SQUID magnetometer with additional positive feedback," *Rev. Sci. Instrum.* **66**, 3008–3015 (1995).
24. C. Johnson, P. D. D. Schwindt, and M. Weisend, "Magnetoencephalography with a two-color pump-probe, fiber-coupled atomic magnetometer," *Appl. Phys. Lett.* **97**, 243703 (2010).
25. D. Budker, D. F. Kimball, and D. P. DeMille, *Atomic Physics: An Exploration Through Problems and Solutions* (Oxford University, 2004).